Optimal Tuning for Linear and Nonlinear Parameters of Power System Stabilizers in Hybrid System Modeling

Seung-Mook Baek, *Student Member, IEEE,* Jung-Wook Park, *Member, IEEE,* and
Ian A. Hiskens, *Fellow, IEEE*

Abstract-- **This paper focuses on the systematic optimal tuning of a power system stabilizer (PSS), which can improve the system damping performance immediately following a large disturbance. As the PSS consists of both linear parameters, such as the gain and time constant, and non-smooth nonlinear parameters, such as saturation limits of the PSS, two methods are applied to achieve optimal tuning of all parameters. One is to use the optimization technique based on the Hessian matrix estimated by the feed-forward neural network (FFNN), which identifies the first-order derivatives obtained by the trajectory sensitivities, for the nonlinear parameters. The other is to use an eigenvalue analysis for the linear parameters. The performance of parameters optimized by the proposed method is evaluated by time-domain simulation in both a single-machine infinite bus (SMIB) system and a multi-machine power system (MMPS).**

Index Terms—**Eigenvalue analysis, feed-forward neural network, Hessian matrix estimation, hybrid system, nonlinearities, parameter optimization, power system stabilizer, trajectory sensitivities.**

I. INTRODUCTION

IN power systems, the power system stabilizer (PSS) used to mitigate system damping of low-frequency oscillations is an important control objective for optimization design. For the tuning of linear parameters of the PSS such as gain and time constants, the conventional tuning processes [1]-[4] based on the linear approaches such as the eigenvalue analysis have been used. However, by focusing only on small signal condition, the dynamic damping performance immediately following a large disturbance is often degraded. The PSS output limits can provide a solution to balance theses competing effects. In particular, these limit values attempt to prevent the machine terminal voltage from falling below the exciter reference level while the speed is also dropping, which means that it can improve the reduced transient recovery after a disturbance [4]. Non-smooth nonlinear parameters such as the saturation limits of the PSS cannot be tuned by the above linear approaches. On the other hand, the hybrid systems have

recently attracted considerable attention in design of physical systems, which exhibit a mix of continuous, discrete-time and discrete-event dynamics by interactions between linear and nonlinear properties [5], [6]. Especially, a set of the differential-algebraic-impulsive-switched (DAIS) structure [7] for the hybrid system modeling, explicitly provide an effective and insightful analysis of the non-smooth and nonlinear dynamics in power systems. Therefore, it makes possible to implement systematic optimal tuning of nonlinear parameters such as the saturation limit values of the PSS.

In this study, the output limits of the PSS are determined by a nonlinear optimization technique based on the Hessian matrix estimated by the feed-forward neural network (FFNN), which identifies the first-order derivatives obtained by the trajectory sensitivities. The computation of trajectory sensitivities is available from the hybrid system modeling with the DAIS structure. In other words, the FFNN identifier embedded in the hybrid system modeling is used to estimate the second-order derivatives of an objective function **J** with respect to the nonlinear parameters. Thereafter, this Hessian information with the second-order derivatives is effectively applied for the optimal tuning of the saturation output limits. Also, the analysis of the linear parameters of the PSS gives a chance to evaluate the damping performance of low-frequency oscillations based on the small-signal stability. The DAIS based hybrid system modeling enables to form the overall system matrix, which can provide the information of the eigenvalues to decide the appropriate linear parameters. The performances of linear and nonlinear parameters of the PSS tuned by the proposed method are evaluated with case studies on both the SMIB system and the IEEE benchmark four-machine two-area system.

This paper is organized as follows: Section II presents a summary of the hybrid system model with the DAIS structure. Then, the FFNN estimator to approximate the Hessian matrix with the second-order derivatives is described in Section III. The implementation of the proposed method for the optimal tuning of the PSS is described in Section IV. And, the simulation results are given in Section V to evaluate the performance of the proposed method. Finally, conclusions are given in Section VI.

II. Hybrid System Presentation

A. Modeling

As mentioned in Section I, hybrid systems, which include power systems, are characterized by the following:

- Continuous and discrete states.
- Continuous dynamics.
- Discrete events or triggers.
- Mappings that define the evolution of discrete states at events.

In other words, the hybrid system is a mathematical model of physical process consisting of an interacting continuous and discrete event system [7]. A formal presentation of the hybrid system is given in [8], where a general hybrid dynamical system is defined as $H = [Q, \Sigma, A, G]$ and

- Q is the set of discrete states;
- $\Sigma = \{\Sigma_q\}_{q \in Q}$ is the collection of dynamical systems $\Sigma_q = [X_q, \Gamma_q, f_q]$ where each X_q is an arbitrary topological space forming the continuous state space of Σ_q, Γ_q is a semi-group over which the states evolve, and f_q generates the continuous state dynamics;
- $A = \{A_q\}_{q \in Q}$, $A_q \subset X_q$ for each $q \in Q$, is the collection of autonomous jump sets, i.e., the conditions which trigger jumps;
- $G = \{G_q\}_{q \in Q}$, where $G_q: A_q \to S = U_{q \in Q}(X_q \times \{q\})$ is the autonomous jump transition map. The hybrid state-space of H is given by S.

The above level of abstraction of the general hybrid system does not suit the implementation of the numerical optimization method carried out in this study, for which the trajectory sensitivities can be exploited efficiently. A hybrid model with the DAIS structure, which is more conducive to such analysis, can be presented without loss of generalities as follows.

$$\dot{\underline{x}} = \underline{f}(\underline{x}, y) \tag{1}$$

$$0 = g(\underline{x}, y), \tag{2}$$

$$0 = \begin{cases} g^{(i-)}(\underline{x}, y) & y_{d,i} < 0, \\ g^{(i+)}(\underline{x}, y) & y_{d,i} > 0, \end{cases} \quad i = 1, \cdots, d, \tag{3}$$

$$\underline{x}^+ = \underline{h}_j(\underline{x}^-, y^-) \quad y_{e,j} = 0, \quad j \in \{1, \cdots, e\}, \tag{4}$$

where:

$$\underline{x} = \begin{bmatrix} x \\ z \\ \lambda \end{bmatrix}, \quad \underline{f} = \begin{bmatrix} f \\ 0 \\ 0 \end{bmatrix}, \quad \underline{h}_j = \begin{bmatrix} x \\ h_j \\ \lambda \end{bmatrix},$$

$x \in X \subseteq \Re^n, y \in Y \subseteq \Re^m, z \in Z \subseteq \Re^l, \lambda \in L \subseteq \Re^p$,

and

- x represents the continuous dynamic states, for example generator angles, speed, and fluxes in a power system.
- z represents discrete dynamic states, such as transformer tap positions and protection relay logic states.

- y represents algebraic states, e.g. load bus voltage magnitudes and angles.
- λ represents parameters such as generator reactance, controller gains, switching times, and limit values.

The differential equation $\underline{f}$ in (1) is correspondingly structured for $\dot{x} = \underline{f}(\underline{x}, y)$, whilst z and λ remain constant away from events. Similarly, the reset equations $\underline{h}_j$ in (4) ensure that x and λ remain constant at reset events, but the dynamic states z are reset to new values according to z^+ (The notation $\underline{x}^+$ denotes the value of $\underline{x}$ just after the reset event, while $\underline{x}^-$ and y^- refer the values of $\underline{x}$ and y just prior to the event). The algebraic function g in (2) is composed of $g^{(0)}$ together with appropriate choices of $g^{(i-)}$ or $g^{(i+)}$, depending on the signs of the corresponding elements of y_d in (3). An event is triggered by an element of y_d changing sign and/or an element of y_e in (4) passing through zero. In other words, at an event, the composition of g changes and/or elements of z are reset. The system flows ϕ are defined accordingly as

$$\phi(\underline{x}_0, t) = \begin{bmatrix} \phi_{\underline{x}}(\underline{x}_0, t) \\ \phi_y(\underline{x}_0, t) \end{bmatrix} = \begin{bmatrix} x(t) \\ y(t) \end{bmatrix}. \tag{5}$$

A more detailed explanation and associated mathematical equations of the DAIS model (especially for the *switching and impulse effects*) are given in [7] along with comprehensive studies of the hybrid system.

B. Trajectory Sensitivities

The flows ϕ in (5) of a system will generally vary with changes in parameters and/or initial conditions. Trajectory sensitivity provides a way of quantifying the changes in the flow that result from (small) changes to parameters and/or initial conditions. The development of these sensitivity concepts will be based on the DAIS model in (1)~(4). Trajectory sensitivities follow from the Taylor series expansion (neglecting higher order terms) of the flows $\phi_{\underline{x}}$ and ϕ_y in (5), which can be expressed as

$$\Delta \underline{x}(t) = \Delta \phi_{\underline{x}}(\underline{x}_0, t) \approx \frac{\partial \phi_{\underline{x}}(\underline{x}_0, t)}{\partial \underline{x}_0} \Delta \underline{x}_0 \equiv \Gamma_{\underline{x}_0}(t) \Delta \underline{x}_0 \tag{6}$$

$$\Delta y(t) = \Delta \phi_y(\underline{x}_0, t) \approx \frac{\partial \phi_y(\underline{x}_0, t)}{\partial \underline{x}_0} \Delta \underline{x}_0 \equiv \Gamma_y(t) \Delta \underline{x}_0 \tag{7}$$

where $\Gamma_{\underline{x}_0} \in \Re^{n \times \underline{n}}$ and $\Gamma_y \in \Re^{m \times \underline{n}}$ are partial derivatives matrices of system flows and known as the trajectory sensitivities. Recall that $\underline{x}_0$ incorporates the parameters λ, therefore the sensitivities to initial conditions $\underline{x}_0$ include parameter sensitivities. The calculations in (6) and (7) require expensive computational efforts to some degree when the equations have high dimension for large systems. Fortunately, by using an *implicit* numerical integration technique such as

trapezoidal integration, the computational burden for obtaining the trajectory sensitivities can be reduced considerably.

III. FFNN ESTIMATOR EMBEDDED IN HYBRID SYSTEM

In most physical dynamic systems, building the true Hessian is infeasible, as it involves the true second-order trajectory sensitivities, which are computationally expensive. The approximate Hessian can figure out the above problem and may provide an indication of coupling between design parameters, and hence allow physical insights that facilitate the design process. In this paper, the FFNN is applied to estimate the Hessian, which is used in optimization process.

A. Hessian Matrix Estimation by a FFNN

The FFNN based estimator in Fig. 1 is designed to identify the full dynamics of the hybrid system, which are both the system flows in (5) and the trajectory sensitivities in (6) and (7). Thereafter, it validates the system model with its converged weights and estimates the second-order derivatives of a user-defined objective function $\mathbf{J}$ with respect to the nonlinear parameters to be optimized. The FFNN (with the multilayer perceptron structure [9]) consists of three-layers of neurons (input, hidden, and output layer) interconnected by the weight matrices $\mathbf{W}_l$ and $\mathbf{W}_L$ (see the Fig. 2 in [9]), and it is first trained to identify the dynamics of the plant. Generally, because the FFNN starts with random initial values for its weights, and then computes a one-pass backpropagation algorithm at each time step k, which consists of a forward pass propagating the input vector through the network layer by layer, and a backward pass to update the weights with the error signal between $[\partial \mathbf{J}/\partial \lambda_i, \partial \mathbf{J}/\partial \lambda_j]$ and $[\partial \widetilde{\mathbf{J}}/\partial \lambda_i, \partial \widetilde{\mathbf{J}}/\partial \lambda_j]$ as shown in Fig. 1.
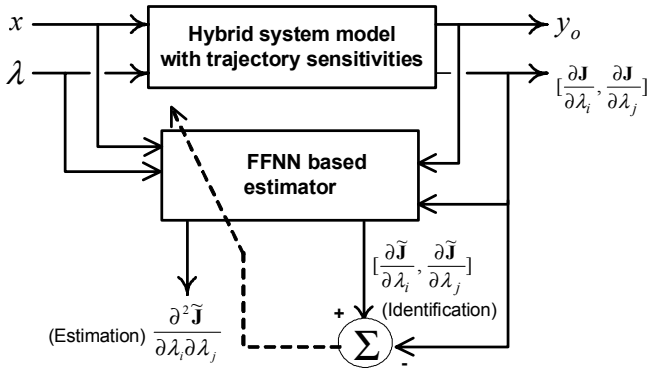

Fig. 1. FFNN applied to the hybrid system.

The objective function $\mathbf{J}$ in the optimization process can be normally defined as a positive and quadratic form, therefore, its derivative exists. With the identified gradient $\nabla \widetilde{\mathbf{J}}$ in Fig. 1, the second-order derivatives $\nabla^2 \widetilde{\mathbf{J}}$ can be estimated by the one-step backpropagation computation in (8). Also, its associated Hessian matrix $\widetilde{\mathbf{H}}$ is expressed by (9). Implementation for the minimization of the objective function $\mathbf{J}$ and the trajectory sensitivities $\nabla \mathbf{J}$ in the DAIS structure is explained in the Section IV.

$$\nabla^2 \widetilde{\mathbf{J}} = \frac{\partial^2 \widetilde{\mathbf{J}}}{\partial \lambda_i \partial \lambda_j} = \frac{\partial \nabla \widetilde{\mathbf{J}}}{\partial p_L} \frac{\partial p_L}{\partial q_L} \frac{\partial q_L}{\partial p_l} \frac{\partial p_l}{\partial q_l} \frac{\partial q_l}{\partial \lambda_j} = \frac{\partial \widetilde{\mathbf{\Gamma}}_{(x,y)}}{\partial p_L} \frac{\partial p_L}{\partial q_L} \frac{\partial q_L}{\partial p_l} \frac{\partial p_l}{\partial q_l} \frac{\partial q_l}{\partial \lambda_j}$$

$$= \left\{ s(q_l)(1 - s(q_l)) \mathbf{W}_l(\lambda_j) \right\} \sum_{j=1}^{m_l} \widetilde{\mathbf{\Gamma}}_{(x,y)} \cdot \mathbf{W}_L$$

(8)

where m_l is the number of neurons in the hidden layer; p is the output of the activation function for a neuron; q is the regression vector as the activity of a neuron; $\mathbf{W}$ is the weight matrix; L and l denote the output and hidden layer, respectively; $\nabla \widetilde{\mathbf{J}}$ is the trajectory sensitivities identified by FFNN ($\nabla \widetilde{\mathbf{J}} = \widetilde{\mathbf{\Gamma}}_{(x,y)}$); The function s in (8) is the sigmoidal function given as $s(x) = 1/\{1 + \exp(-x)\}$.

$$\widetilde{\mathbf{H}}(\lambda) = \begin{bmatrix} \partial^2 \widetilde{\mathbf{J}}/\partial \lambda_i^2 & \partial^2 \widetilde{\mathbf{J}}/\partial \lambda_i \partial \lambda_j \\ \partial^2 \widetilde{\mathbf{J}}/\partial \lambda_j \partial \lambda_i & \partial^2 \widetilde{\mathbf{J}}/\partial \lambda_j^2 \end{bmatrix} \quad (9)$$

B. Example: Application to a Switched Hybrid System

The system description [7] is $\dot{x} = A_i x$,

where $A_1 = \begin{bmatrix} 1 & -100 \\ 10 & 1 \end{bmatrix}$, $A_2 = \begin{bmatrix} 1 & 10 \\ -100 & 1 \end{bmatrix}$

The index i changes from 1 to 2 when $x_2 = 2.75 \cdot x_1$ and from 2 to 1 when $x_2 = 0.32 \cdot x_1$. Initially, $x_0 = [1\ 1]^t$ and $i = 1$. This model can be written in the DAIS form in (1) ~ (4) as

$$\dot{x} = \begin{bmatrix} 1 & z_1 \\ z_2 & 1 \end{bmatrix} x$$

$$0 = \begin{cases} \lambda_1 x_1 - x_2 - z_3 y, & y < 0 \\ x_2 - \lambda_2 x_1 - z_3 y, & y > 0 \end{cases}$$

$$\left. \begin{array}{l} z_1^+ = z_2^- \\ z_2^+ = z_1^- \\ z_3^+ = -z_3^- \end{array} \right\}, \quad \text{when} \quad y = 0$$

where $\underline{x}_0 = [x_0\ z_0\ \lambda]^t = [1\ 1\ -100\ 10\ 1\ 2.75\ 0.32]^t$ ($x_0 = [1\ 1]^t$, $z_0 = [-100\ 10\ 1]^t$, $\lambda = [2.75\ 0.32]^t$) and $y_0 = -1$.
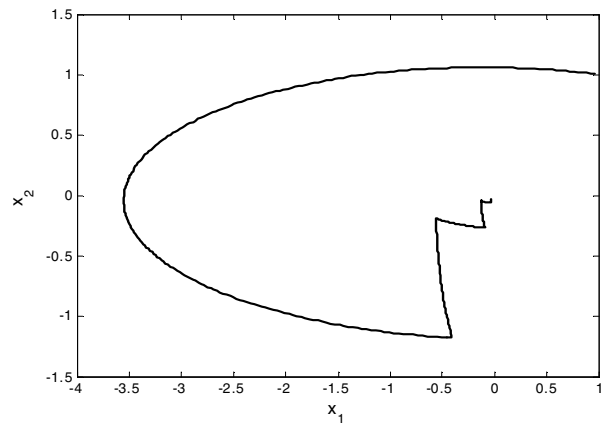

Fig. 2. Phase portraits for the hybrid system in the example.

The phase portrait is shown in Fig. 2. The change between A_1 and A_2 in the above example is achieved by resetting the matrix elements z_1 and z_2 whenever a switching surface is encountered. This example gives a good illustration for the fact that the two unstable sub-systems (the eigenvalues of both A_1 and A_2 are equal to $\lambda = 1 \pm j\omega_0$ where $\omega_0 = \sqrt{1000}$) can make the overall system stable through the proper switching action by the hybrid system modeling, independently of the initial states (which means that this hybrid system is guaranteed to be asymptotically stable).

Assume that the FFNN estimator is designed to identify the objective function $\mathbf{J} = (x_1^4 + x_2^3 + 4x_1 x_2)$ and its partial derivatives with respect to states x_1 and x_2, which are $\partial \mathbf{J} / \partial x_1 = (4x_1^3 + 4x_2)$ and $\partial \mathbf{J} / \partial x_2 = (3x_2^2 + 4x_1)$. After taking the necessary steps (training→testing→fixed weights), the good identification performance of the first-order derivatives by the FFNN with sufficient accuracy (even when the on-line training is stopped) is shown in Fig. 3. Thereafter, it estimates the second-order derivatives, which are $\partial^2 \mathbf{J} / \partial x_1^2 = 12 x_1^2$ and $\partial^2 \mathbf{J} / \partial x_2^2 = 6 x_2$ by using (8). The results are shown in Fig. 4. The FFNN approximates the second-order partial derivatives of this hybrid system with acceptable accuracy, which can be used to apply the numerical optimization technique.
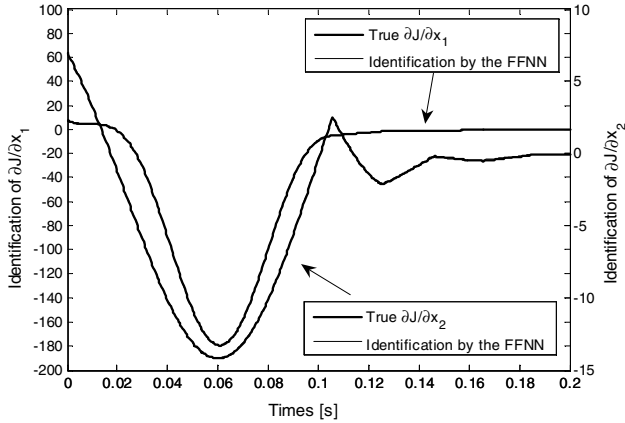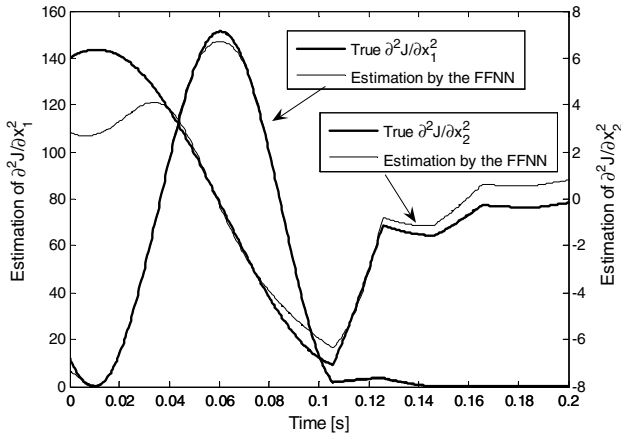

Fig. 3. Identification performance of the FFNN.

Fig. 4. Estimation of the second-order partial derivatives by the FFNN.

IV. IMPLEMENTATION OF OPTIMAL TUNING FOR LINEAR AND NONLINEAR PARAMETERS OF PSS

A. Modeling and Implementation Procedure

Figure 5 shows the control block diagram of generator's excitation system with the PSS and automatic voltage regulator (AVR)/Exciter. The modeling by the DAIS structure for the PSS output limits and AVR anti-windup limits in Fig. 5 is given in (10) and (11), respectively. More detailed explanations for the hybrid system modeling of a SMIB system including the generator are given in [10].
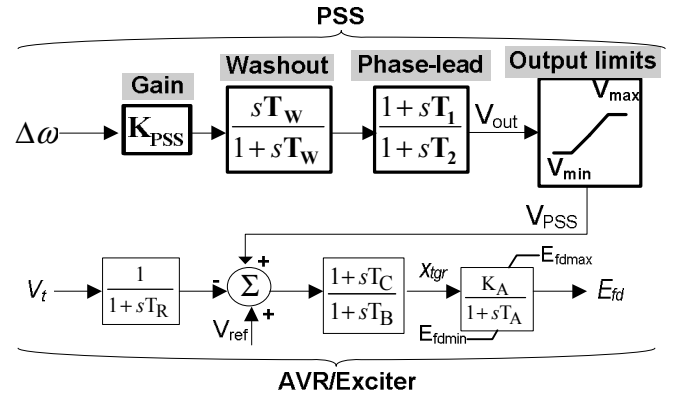

Fig. 5. PSS/AVR block representation.

$$y_1 = V_{max} - V_{out};$$
$$y_2 = V_{out} - V_{min}; \tag{10}$$

$$0 = \begin{cases} g_1^{(i-)}(\underline{x}, y) = V_{PSS} - V_{max} & y_1 < 0, \\ g_2^{(i-)}(\underline{x}, y) = V_{PSS} - V_{min} & y_2 < 0, \\ g_1^{(i+)}(\underline{x}, y) = g_2^{(i+)}(\underline{x}, y) = V_{PSS} - V_{out} & y_1 > 0, y_2 > 0. \end{cases}$$

$$y_3 = E_{fdmax} - E_{fd}; \quad y_4 (\text{upper limits switch}) : (+ \text{when } y_3 < 0)$$
$$y_5 = E_{fd} - E_{fdmin}; \quad y_6 (\text{lower limits switch}) : (+ \text{when } y_5 < 0)$$

$$0 = \begin{cases} g_3^{(i-)}(\underline{x}, y) = y_4 - 1 & y_3 < 0, \\ g_4^{(i-)}(\underline{x}, y) = E_{fd} - E_{fdmax} & y_3 < 0, \\ g_5^{(i-)}(\underline{x}, y) = y_6 - 1 & y_5 < 0, \\ g_6^{(i-)}(\underline{x}, y) = E_{fd} - E_{fdmin} & y_5 < 0, \\ g_3^{(i+)}(\underline{x}, y) = g_5^{(i+)}(\underline{x}, y) = y_4 = y_6 & y_3 > 0, y_5 > 0, \\ g_4^{(i+)}(\underline{x}, y) = g_6^{(i+)}(\underline{x}, y) = K_A \cdot x_{trg} - E_{fd} & y_3 > 0, y_5 > 0. \end{cases} \tag{11}$$

For the optimal tuning of the PSS in Fig. 5, the steps in Fig. 6 are taken to implement both the linear and nonlinear parameters optimization. Firstly, the nonlinear parameters (V_{max} and V_{min} in Fig.5, which are the saturation upper and lower limits) of the PSS are determined by applying the numerical optimization technique with the estimated Hessian matrix in (9). Then, the linear parameters (K_{pss}, T_w, T_1 and T_2 in Fig. 5) of the PSS are properly selected by the eigenvalue analysis of the system matrix **A** built from the DAIS modeling. Therefore, the PSS tuned optimally for all parameters can provide the overall robustness for the large and small

disturbances to the system. The detailed descriptions for their implementation are given in the next sub-sections.
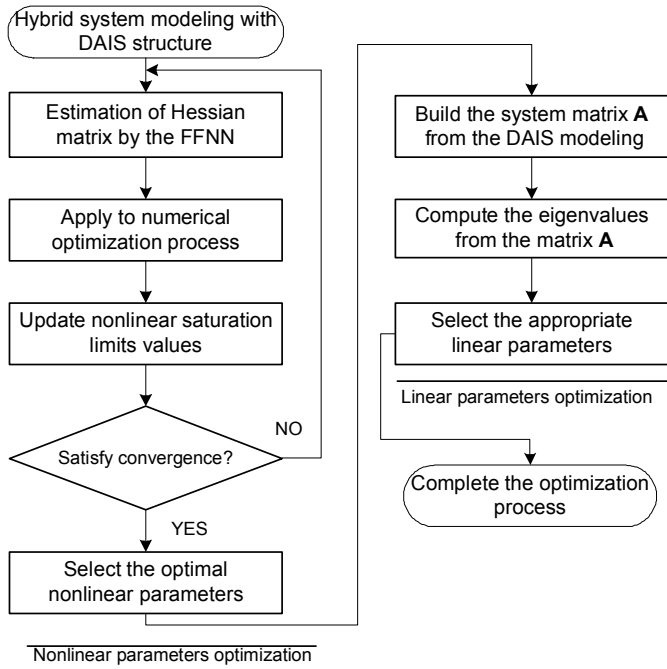

Fig. 6. Procedure to implement the parameter optimization of the PSS.

B. Nonlinear Parameter Optimization by FFNN Identifier

Many practical optimization problems can be formulated by using a Bolza form of the objective function $\mathbf{J}$

$$\min_{\lambda, t_f} \mathbf{J}(\underline{x}, y, \lambda, t_f) \qquad (12)$$

subject to $\begin{bmatrix} \underline{x}(t) \\ y(t) \end{bmatrix} = \phi(\underline{x}_0, t)$ in (5), and

$$\mathbf{J} = \varphi\left(\underline{x}(t_f), y(t_f), \lambda, t_f\right) + \int_{t_0}^{t_f} \psi(\underline{x}(t), y(t), \lambda, t) dt. \qquad (13)$$

In (13), λ represents the optimized parameters (output limits of the PSS in Fig. 5), which are adjusted to minimize the value of objective function $\mathbf{J}$, and t_f is the final time. Also, φ is the cost or penalty associated with the error in the terminal state at time t_f, and ψ is the cost function associated with transient state errors. The PSS is used to mitigate system damping and force the system to recover to the post-disturbance stable operating point as quickly as possible. The speed deviation ($\Delta\omega$) and terminal voltage deviation (ΔV_t) of the generator in a power system are considered to be good assessments of the damping and recovery [1]. Therefore, the objective function $\mathbf{J}$ in (13) can be re-formulated for the optimal tuning of the PSS with specific final time t_f as the follows

$$\mathbf{J}(\lambda) = \int_{t_0}^{t_f}\left(\begin{bmatrix} \omega(\lambda, t) - \omega^s \\ V_t(\lambda, t) - V_t^s \end{bmatrix}^T \mathbf{V} \begin{bmatrix} \omega(\lambda, t) - \omega^s \\ V_t(\lambda, t) - V_t^s \end{bmatrix}\right) dt, \qquad (14)$$

where $\mathbf{V}$ is the diagonal matrix with weighting factors.

The ω^s and V_t^s are the post-fault steady state values of ω and V_t, respectively. Minimization of the value of $\mathbf{J}$ in (14) is straightforward even though the cost is obtained by integrating over the system flows (trajectories). The simplest way of obtaining $\mathbf{J}$ is to introduce a new state variable $\underline{x}_{\text{cost}}$, with $\dot{\underline{x}}_{\text{cost}}$ equal to the integrand of (14). Thereafter, $\underline{x}_{\text{cost}}(t_f) = \mathbf{J}$. The trajectory sensitivities with respect to λ directly provide the gradient by

$$\nabla \mathbf{J} = \mathbf{\Gamma}_{\underline{x}_{\text{cost}}}(t_f). \qquad (15)$$

While identifying the $\nabla \mathbf{J}$ in (15) by the FFNN, the Hessian matrix $\widetilde{\mathbf{H}}$ is estimated by the computation in (8) and (9). Then, during the optimization process, these nonlinear parameters λ are updated by using (16) at each iteration k until its convergence is satisfied.

$$\lambda_{k+1} = \lambda_k + \alpha \cdot \widetilde{\mathbf{H}}^{-1}(\lambda) \cdot \nabla \mathbf{J}(\lambda) \qquad (16)$$

where α is the step-length to ensure that the optimal path (search) is the descent direction vector.

C. Linear Parameter Optimization by Eigenvalue Analysis

Small-signal stability is the ability of the power system to maintain synchronism when subjected to small disturbances [4]. The use of linear techniques for the small-signal stability provides the valuable information about the inherent dynamic characteristics of the system and assists in the proper selection of linear parameters. In this study, the PSS linear parameters (K_{pss}, T_w, T_1 and T_2 in Fig. 5) are determined by the eigenvalue analysis.

As mentioned before, the trajectory sensitivity, which are the partial derivatives of f and g with respect to the total dynamic and algebraic variables ($\underline{x}$ and y), can be accurately computed based on the DAIS structure in (1)~(7). Thereafter, the eigenvalues of the overall system can be obtained from the system matrix $\mathbf{A}$ with the reduced order in (17).

$$\begin{aligned} \Delta \dot{\underline{x}} &= \underline{f}_{\underline{x}} \cdot \Delta \underline{x} + \underline{f}_y \cdot \Delta y, \\ 0 &= g_{\underline{x}} \cdot \Delta \underline{x} + g_y \cdot \Delta y \\ \Delta y &= -g_y^{-1} \cdot g_{\underline{x}} \cdot \Delta \underline{x}, \ \Delta \dot{\underline{x}} \\ &= (\underline{f}_{\underline{x}} - \underline{f}_y \cdot g_y^{-1} \cdot g_{\underline{x}}) \cdot \Delta \underline{x} = \mathbf{A} \cdot \Delta \underline{x} \end{aligned} \qquad (17)$$

V. CASE STUDIES

A. Test in SMIB System

The SMIB system is shown in Fig. 7. The excitation system in Fig. 5 is connected to the generator ($\mathbf{G}$) of the SMIB system. The generator ($\mathbf{G}$) is accurately represented by a six-order machine model, viz., a two-axis (d-q) model with two damper windings in each axis [11].
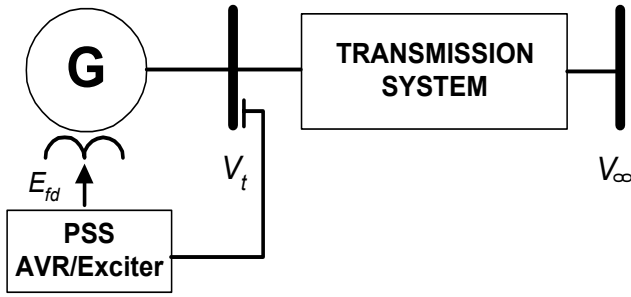
Fig. 7. Single-machine infinite bus (SMIB) system.

With the values of $\nabla \mathbf{J}$ in (15), the FFNN estimator consists of the 7 inputs (threshold input of 1, $\Delta\omega$, ΔV_t, V_{max}, V_{min}, $\partial \mathbf{J}/\partial V_{max}$, $\partial \mathbf{J}/\partial V_{min}$) and the 10 neurons in the hidden layer. As shown in Fig. 1, the FFNN outputs the $\partial \widetilde{\mathbf{J}}/\partial V_{max}$ and $\partial \widetilde{\mathbf{J}}/\partial V_{min}$, which identifies the true trajectory sensitivities. Thereafter, it computes the estimated Hessian $\widetilde{\mathbf{H}}$ by using (8) and (9), which are the approximate second-order derivatives with respect to the nonlinear parameters λ, with its converged weights.

To evaluate the performance of the PSS tuned by the proposed method, the SMIB system in Fig. 7 is now disturbed by applying a 200 ms three-phase short circuit fault with the fault-impedance of 0.05 pu to the generator terminal bus at 0.1 s. The convergence performances during the optimization process by (16) are shown in Figs. 8 and 9 with comparison of those by the well-known steepest descent algorithm [12] in (18) for the value of $\mathbf{J}$ and maximum relative gradient $f_{r\text{-}gradient}$ in (19). For the fair comparison, the same value of the fixed step-length $\alpha\,(=0.22)$ is used in (16) and (18).

$$\lambda_{k+1} = \lambda_k + \alpha \cdot \nabla \mathbf{J}(\lambda) \qquad (18)$$

$$
\begin{aligned}
f_{r-gradient} &= \left\| \frac{\text{relative rate of change in } \mathbf{J}}{\text{relative rate of change in } \underline{x}} \right\|_\infty \\
&= \left\| \frac{\nabla \mathbf{J}(\underline{x}_k) \cdot \underline{x}_k}{\mathbf{J}(\underline{x}_k)} \right\|_\infty
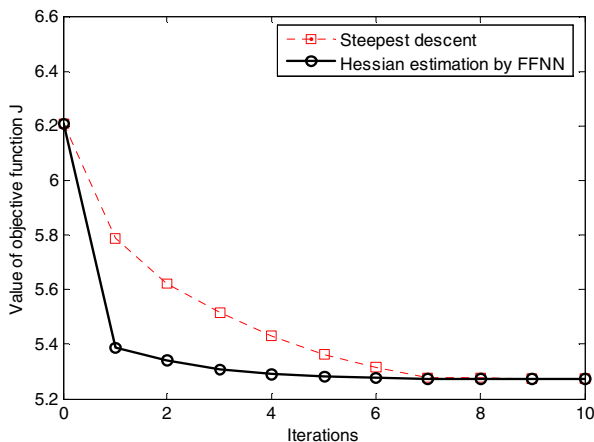\end{aligned}
\qquad (19)
$$

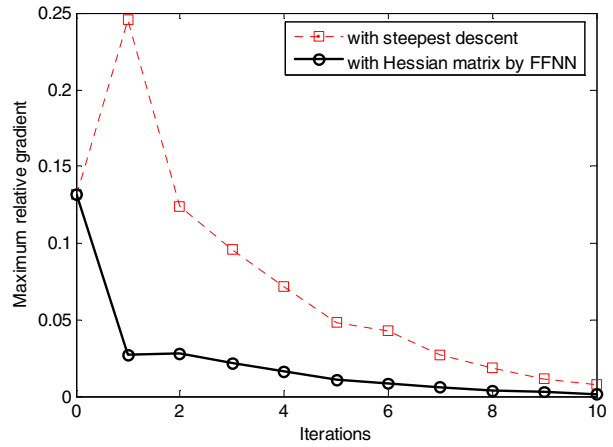Fig. 8. Minimization of the objective function $\mathbf{J}$.

Fig. 9. Maximum relative gradient variations.

It is clearly shown from the results that the proposed method by the estimated Hessian improves the convergence speed very effectively. In other words, the values of both $\mathbf{J}$ and $f_{r\text{-}gradient}$ almost converge after only 5 iterations when the optimization process is implemented by the proposed method. The value of V_{max} has been changed a litter from 0.1 to 0.1109, but the value of V_{min} has moved significantly from –0.1 to – 0.3317 at 5 iterations.

Thereafter, the linear parameters are selected to give more damping to the system by the eigenvalue analysis with the system matrix $\mathbf{A}$ obtained from (17). Note that the optimized nonlinear parameters λ are fixed when the linear parameters are considered. The results are given in Table I. The eigenvalue given in Table I corresponds to the speed deviation ($\Delta\omega$) mode of the generator, which assesses the system damping of low-frequency oscillation. The real part of the eigenvalue has been changed from -1.67 to -5.17, which means that the value of damping ratio by the optimal parameters is three times greater than that by the initial linear parameters. Therefore, it is expected that the optimal parameters can improve the system damping performance more effectively than the initial ones.

The rotor angle and speed deviation responses are shown in Figs. 10 and 11, respectively. The effect of optimal tuning for nonlinear saturation limits is rather dramatic and quite evident for a large disturbance (such as a three-phase short circuit applied to a power system. Also, the linear parameters provide the effective damping and fast recovery after the second swing, which is relatively more stable condition when compared to the first swing.

TABLE I
INITIAL VS. OPTIMAL LINEAR AND NONLINEAR VALUES OF PSS IN SMIB

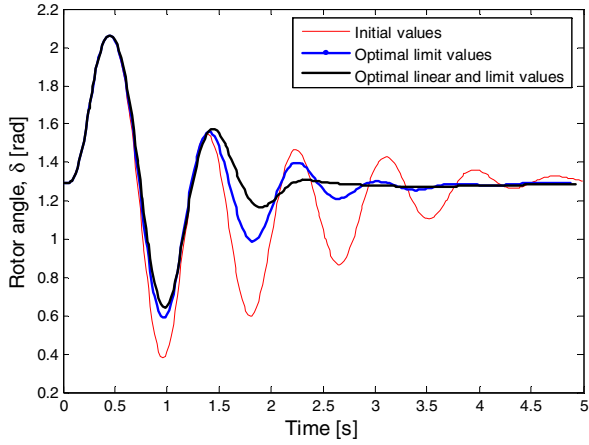| Values of PSS	Nonlinear		Linear				Eigen-values
	V_{max}	V_{min}	K_{pss}	T_w	T_1	T_2	
Initial	0.1	-0.1	2	10	5	0.05	-1.69± j8.28
Optimal	0.1109	-0.3317	5.5	10.2	3.5	0.005	-5.17± j9.66

1670

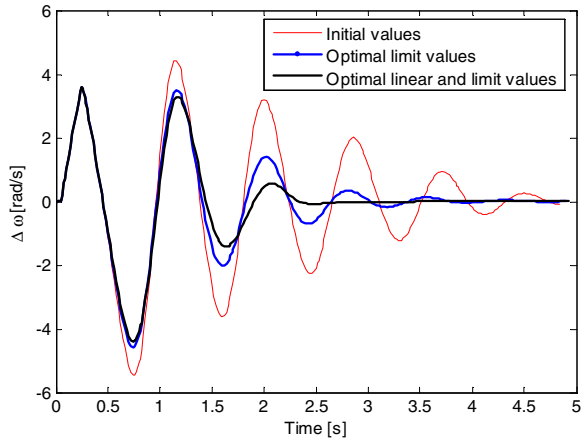Fig. 10. Generator rotor angle response [rad].

Fig. 11. Speed deviation response [rad/s] in generator.

B. Test in Multi-Machine Power System

The IEEE benchmark four-machines, two-area test system is shown in Fig. 12. The data of this system are given in [4]. Each machine has been represented by the fourth-order nonlinear model [11]. All generators (G1~G4) are equipped with the excitation system shown in Fig. 5.
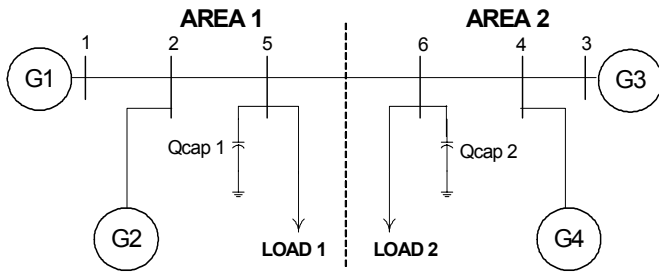

Fig. 12. IEEE benchmark four-machine two-area test system.

The effect of the optimal linear and nonlinear parameter values of the multi-PSSs on the MMPS in Fig. 12 with respect to the damping performance is investigated. Firstly, for the optimal tuning of the nonlinear parameters, the objective function **J** in (14) is re-defined for the application to the MMPS as

$$\mathbf{J}(\lambda) = \sum_{i=1}^{4} \int_{t_0}^{t_f} \left(\begin{bmatrix} \omega_i(\lambda,t) - \omega_i^s \\ V_{t,i}(\lambda,t) - V_{t,i}^s \end{bmatrix}^T \mathbf{V} \begin{bmatrix} \omega_i(\lambda,t) - \omega_i^s \\ V_{t,i}(\lambda,t) - V_{t,i}^s \end{bmatrix} \right) dt, \quad (20)$$

where the subscript i is the generator number in Fig. 12. While minimizing the single value of **J** in (20), the FFNN estimators are applied to determine the optimal saturation limits of the separate PSS in each generator, which are affected by the interactions of each other on the MMPS. For each FFNN estimator, the all 7 inputs and 10 neurons are used in the input and hidden layers, respectively. Then, this separate FFNNs estimate the four different Hessian matrices $\tilde{\mathbf{H}}$ (of 2×2 size), which are positive definite, during the optimization process.

Similarly to case study on the SMIB system, the MMPS in Fig. 12 is disturbed by applying a 200 ms three-phase short circuit fault with the fault-impedance of 0.003 pu at bus 6 at 0.1 s. the successfully minimized variations of the function **J**, which corresponded to the nonlinear parameters updated by (16), are shown in Fig. 13.
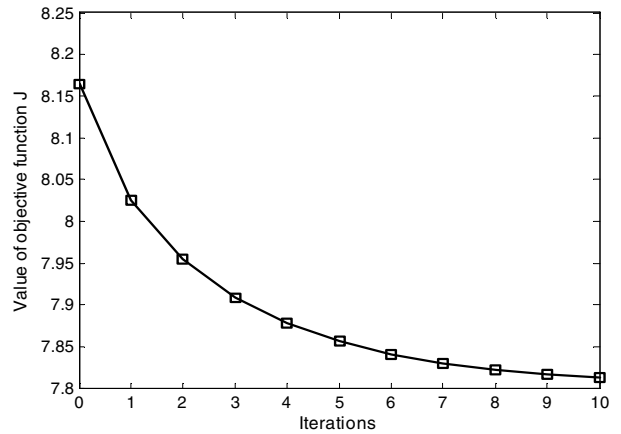

Fig. 13. Variation of the objective function **J**: test on the MMPS.

Subsequently, the total 16 linear parameters of all the PSSs are determined by checking out the eigenvalues, which correspond to the relative speed oscillation modes ($\Delta\omega_1$-$\Delta\omega_2$ in AREA 1 and $\Delta\omega_3$-$\Delta\omega_4$ in AREA 2 in Fig.12), with the system matrix **A** built by (17). The initial and optimal values of the linear parameters are given in Tables II and III, respectively, including those of the nonlinear parameters determined after the tenth iteration.

TABLE II
INITIAL LINEAR AND NONLINEAR VALUES OF PSSs IN MMPS

Initial values	Nonlinear		Linear				Eigen-values
	V_{max}	V_{min}	K_{pss}	T_w	T_1	T_2	
PSS-G1	0.05	-0.05	1	12	2.5	0.05	-2.03± j3.92 (AREA 1)
PSS-G2	0.05	-0.05	1	12	2.5	0.05	
PSS-G3	0.1	-0.1	1	12	4.5	0.05	-1.23± j3.72 (AREA 2)
PSS-G4	0.1	-0.1	1	12	2.5	0.05	

Optimal values	Nonlinear		Linear				Eigen-values
	V_{max}	V_{min}	K_{pss}	T_w	T_1	T_2	
PSS-G1	0.0825	-0.1078	1.2	22.2	4.4	0.029	-10.46± j3.15 (AREA 1)
PSS-G2	0.0503	-0.0490	1.2	20.1	5.1	0.024	
PSS-G3	0.2319	-0.2300	1.3	16.8	4.2	0.032	-2.54± j4.96 (AREA 2)
PSS-G4	0.2457	-0.2466	1.5	17.7	3.7	0.045	

The responses of relative speed oscillations ($\Delta\omega_1$-$\Delta\omega_2$ and $\Delta\omega_3$-$\Delta\omega_4$) in AREA 1 and 2 are shown in Figs. 14 and 15, respectively. The dynamic damping performance is effectively improved by the optimized nonlinear parameters of the PSSs. Note that the optimal saturation limits of the PSSs in AREA 2 have a remarkable effect on damping improvement when compare to those of the PSSs in AREA 1. Correspondingly, the nonlinear parameter variations in AREA 2 are higher than those in AREA 1 (see Tables II and III).

Also, the optimal linear parameters give the additional damping to the power system effectively after the first swing.
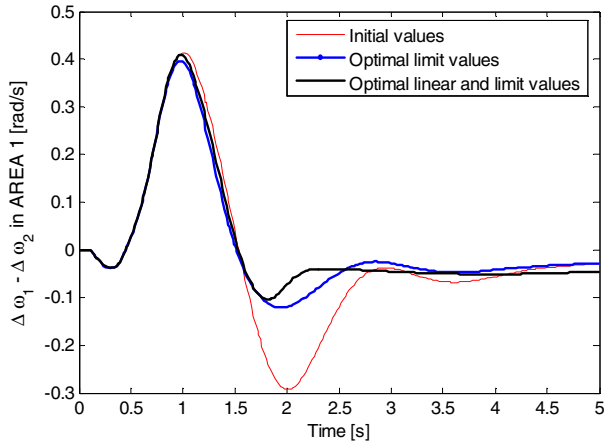

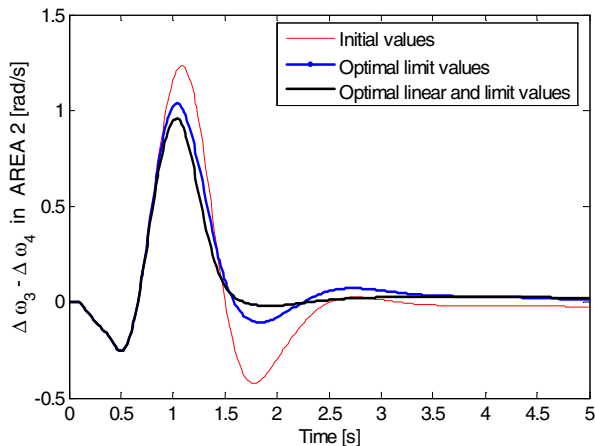Fig. 14. Relative speed oscillations ($\Delta\omega_1$-$\Delta\omega_2$) in AREA 1 [rad/s].

Fig. 15. Relative speed oscillations ($\Delta\omega_3$-$\Delta\omega_4$) in AREA 2 [rad/s].

VI. CONCLUSIONS

In this paper, the linear and nonlinear parameters of the power system stabilizers (PSSs) in power systems were considered as parameters to be optimized by using the hybrid system model with the differential-algebraic-impulsive-switched (DAIS) structure. For optimal tuning for those parameters, two methods were applied. To implement nonlinear parameter optimization, the feedforward neural network (FFNN) was applied to estimate the second-order derivatives of the objective function **J** with respect to the saturation limits with the gradients obtained by the trajectory sensitivities. To select proper linear parameters such as the gain and time constants of the PSS, the eigenvalue analysis was used by the overall system matrix **A**, which can be easily formed with the DAIS structure. Consequently, the damping performances of low-frequency oscillations were effectively improved with those parameters optimized by applying above linear and nonlinear techniques.

VII. REFERENCES

[1] P. Kundur, M. Klein, G.J. Rogers, and M.S. Zywno, "Application of Power System Stabilizers for Enhancement of Overall System Stability," *IEEE Trans. on Power Systems*, Vol.4, No.2, pp. 614-626, May 1989.

[2] M. Klein, G. J. Rogers, S. Moorty, and P. Kundur, "Analytical Investigation of Factors Influencing Power System Stabilizers Performance", *IEEE Trans. on Energy Conversion,* Vol. 7, No. 3, pp. 382-388, September 1992.

[3] N. Martins and L. T. G. Lima, "Determination of Suitable Locations for Power System Stabilizers and Static VAr Compensators for Damping Electromechanical Oscillations in Large Scale Power Systems", *in Proc. of Power Industry Computer Application*, pp.74-82, May 1989.

[4] Prabha Kundur, Power system stability and Control, EPRI Editors, McGraw-Hill, Inc. 1993, ISBN 0-07-035958-X.

[5] A. van der Schaft and H. Schumacher, An Introduction to Hybrid Dynamical Systems, Springer-Verlag, London, 2000.

[6] D. Liberzon, Switching in Systems and Control, Birkhauser, Boston, 2003.

[7] Ian A. Hiskens and M. A. Pai, "Trajectory Sensitivity Analysis of Hybrid Systems", *IEEE Trans. on Circuits and Systems-Part I: Fundamental Theory and Applications*, Vol.47, No.2, pp. 204-220, February 2000.

[8] M. S. Branicky, V. S. Borkar, and S. K. Mitter, " A Unified Framework for Hybrid Control: Model and Optimal Control Theory", *IEEE Trans. on Automat. Contr.,* Vol. 43, pp. 31-45, January 1998.

[9] Jung-Wook Park, G.K. Venayagamoorthy, and R.G. Harley, "MLP/RBF Neural-Networks-Based Online Global Model Identification of Synchronous Generator", *IEEE Transactions on Industrial Electronics*, Vol.52, No. 6. pp. 1685-1695, December 2005.

[10] Ian A. Hiskens and Peter J. Sokolowski, "Systematic Modeling and Symbolically Assisted Simulation of Power Systems", *IEEE Trans. on Power Systems*, vol.16, no.2, pp. 229-234, May 2001.

[11] P. W Sauer and M. A Pai, Power System Dynamics and Stability. Englewood Cliffs, NJ: Prentice-Wall, 1998.

[12] J. Nocedal and S. J. Wright, ed., Numerical Optimization, Springer-Verlag, New York, 1999.